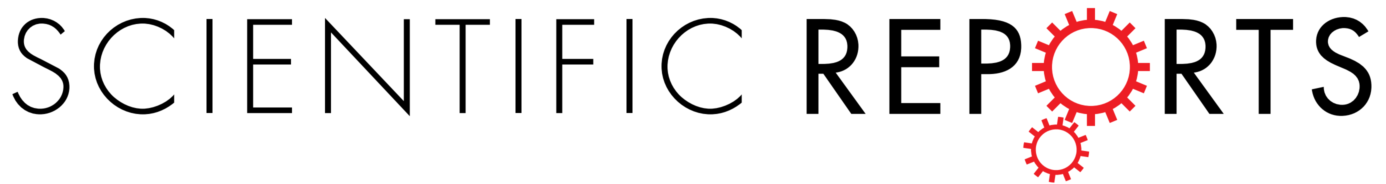

OPEN

Carrier-induced transient defect mechanism for non-radiative recombination in InGaN light-emitting devices

Received: 26 February 2016
Accepted: 11 March 2016
Published: 14 April 2016

Junhyeok Bang[1,2], Y. Y. Sun[1], Jung-Hoon Song[3] & S. B. Zhang[1]

Non-radiative recombination (NRR) of excited carriers poses a serious challenge to optoelectronic device efficiency. Understanding the mechanism is thus crucial to defect physics and technological applications. Here, by using first-principles calculations, we propose a new NRR mechanism, where excited carriers recombine via a Frenkel-pair (FP) defect formation. While in the ground state the FP is high in energy and is unlikely to form, in the electronic excited states its formation is enabled by a strong electron-phonon coupling of the excited carriers. This NRR mechanism is expected to be general for wide-gap semiconductors, rather than being limited to InGaN-based light emitting devices.

Nonradiative recombination (NRR) refers to physical processes in semiconductors under electrical or optical excitations, where electrons and holes recombine without emitting photons. NRR is currently the most important factor limiting the efficiency of optoelectronic and photovoltaic devices in energy applications[1,2]. A good example is the efficiency loss in white light-emitting diodes (LEDs) based on GaN and its alloys[3–10]. The white LEDs hold great promises to revolutionize current lighting technology[11,12]. Their efficiencies, however, are still not enough to penetrate the general lighting market, which is currently dominated by cheep compact fluorescent lamps. Revealing the physics of NRR in such devices is therefore critical to fostering new technology breakthroughs.

The field of NRR study is dominated by the widely-accepted Shockley-Read-Hall (SRH)[13,14] model and the Auger recombination (AR) model[1,4–6]. In the SRH model, defect with deep levels inside the band gap assist carrier recombination such that the energy of the excited carriers is dissipated through lattice vibration or phonon emission. In recent years, other defect-specific NRR processes have also been proposed[15,16]. In the AR process, in contrast, the carrier recombination is mediated by carrier-carrier scattering and the energy is transferred by generating higher energy carriers inside bulk energy continuum, which is then dissipated through phonon emission. The two models can be characterized as a defect centric model and a defect-free model, which has been the paradigm for NRR study over decades.

In this work, we show that the formation of defects, especially the Frenkel-pair (FP) defects, due to the presence of excited carriers creates a new type of NRR centers. The energy of the carriers is dissipated through a transient defect generation and annihilation process. In other words, it starts and ends with no deep level inside the band gap as opposed to the SRH mechanism, but the involvement of the transient defects makes it fundamentally different from the AR. Using first-principles calculations we found that in InGaN, the carrier-induced transient FP formation and associated NRR process can readily take place and compete effectively with radiative recombination. The transient nature of the NRR defects may have made them escape experimental detection, which is largely framed by the current thinking and lack of sub-ns-to-ns time resolutions.

To be more specific, first let us discuss the concept behind the carrier-induced transient-defect NRR. In a typical binary semiconductor, such as GaN, the top part of the valence band (VB) mainly consists of anion-derived bonding states, while the bottom part of the conduction band (CB) mainly consists of cation-derived anti-bonding states[17,18]. Figure 1(a) shows the initial occupations of the electronic states under carrier injection, e.g., in the active region of a working LED, where electrons and holes establish their respective quasi-equilibria at the VB and CB. When an anion is displaced from its original lattice site to an interstitial site, a Frenkel pair (FP) defect (i.e.

[1]Department of Physics, Applied Physics & Astronomy, Rensselaer Polytechnic Institute, Troy, NY 12180, USA. [2]Spin Engineering Physics Team, Korea Basic Science Institute (KBSI), Daejeon 305-806, South Korea. [3]182 Shingwan, Department of Physics, Kongju National University, Kongju Chungnam 314-701, South Korea. Correspondence and requests for materials should be addressed to S.B.Z. (email: zhangs9@rpi.edu)

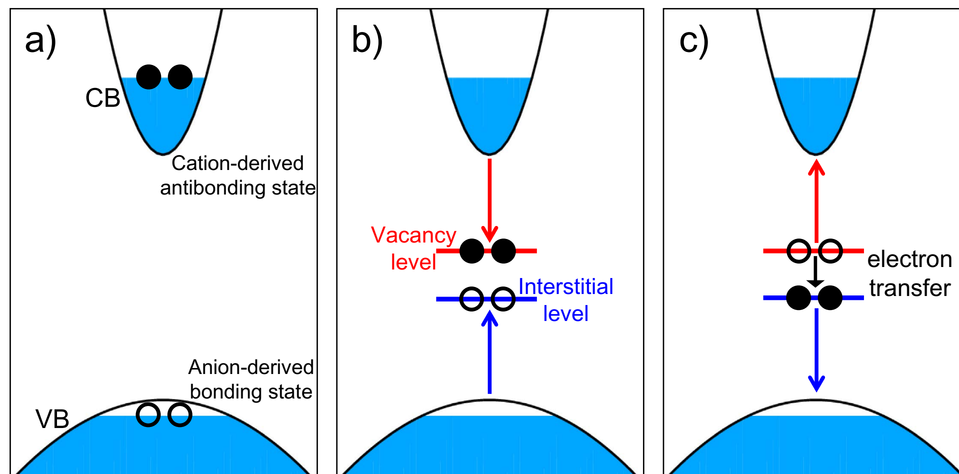

Figure 1. Schematic illustration of the change of the energy levels during NRR. (**a**) Initial defect-free state with injected carriers, (**b**) during FP formation, and (**c**) re-healing process back to defect-free ground-state after two-electron transfer. VB and CB denote the valence and conduction bands, respectively. Shaded blue regions represent occupied states. During the FP formation, an anion vacancy level and an anion interstitial level appear inside the band gap. The injected electrons (filled dot) at the highest occupied state in the CB drop to the vacancy level, whereas the injected holes (empty dot) in the VB raise to the interstitial level. After the electron transfer between the vacancy and interstitial levels, these levels undergo a reverse process to retreat back into the VB and CB, respectively.

a pair of anion vacancy and anion interstitial) is created. As the bonds between the anion and cation are broken, an anion-derived bonding state (near the interstitial) and a cation-derived anti-bonding state (near the vacancy) evolve from the VB and CB into the band gap as the interstitial and vacancy levels, respectively, as shown in Fig. 1(b). The interstitial and vacancy levels carry two holes and two electrons, respectively. Once the two levels approach each other inside the band gap, they exchange carriers. After the exchange, the interstitial moves back to annihilate the vacancy and heal the lattice, by which an NRR process is completed [see Fig. 1(c)].

In the ground state, the FP formation is prohibited because it would require a significant amount of energy to break the bonds and to lift up the (doubly-occupied) interstitial level. With excited carriers, however, such a process becomes possible[19] because 1) the electrons in the CB will drop into the vacancy level, which further shifts downward due to FP formation, and 2) the holes in the VB will rise into the interstitial level, which further shifts up due to FP formation. Thus, both excited electrons and holes can offset the energy required in the FP formation process.

Results

Frenkel pair is unstable in ground state. As an alloy, InGaN can have different local structures made of In clusters (with up to four In atoms around a N atom). Since In-N bond is weaker than Ga-N bond, here for simplicity, we consider only the FP formation at a four In cluster (In_4). This is reasonable because from the calculated formation energy of 90 meV, In_4 concentration at a growth temperature of about 750 °C is on the order of $1.6 \times 10^{18}\,cm^{-3}$ for $In_{0.1}Ga_{0.9}N$ samples. Figure 2 shows the atomic structures before and after the FP formation. The FP is formed by displacing the N at center to a neighboring interstitial site, which leaves an N vacancy (V_N) behind. Figure 2(b) shows that the displaced N forms a split-interstitial with a neighboring N atom. This is consistent with the fact that, among isolated N interstitial configurations in GaN, split-interstitial is most stable[20,21]. The calculated FP formation energy is 4.42 eV in the electronic ground state, indicating that this is a forbidden process at room temperature. It also suggests that any FP generated during the NRR process will eventually recombine.

Carrier relaxation in the NRR processes. Figure 3, light gray lines, shows the change of the energy levels during the FP formation assisted by charge carrier injection resulting in excited electrons near the CBM and excited holes near the VBM. One may notice from the figure that, even in defect-free InGaN, band edge energies deviate from their original positions due to occupation of excited states. This unphysical result is a drawback of the hybrid functional methods[22–24]. The errors have been corrected, according to the degree of localization of the states, yielding the red and blue lines in Fig. 3. It shows that when the N is displaced towards the interstitial site, the In-derived V_N level (which can host two electrons) decreases and the N-derived N interstitial (N_i) level (which can host two holes) increases. Insets **a** and **b** in Fig. 3 show the charge density in the seventh configuration for V_N and N_i, respectively, from which we can also see that the V_N gap state, evolved from the CB, has an anti-bonding character in regarding the broken bonds between the In atoms of the vacancy and the displaced N_i. In contrast, the N_i gap state, evolved from the VB, has a bonding character between these states.

Once the FP is formed (i.e., the final configuration in Fig. 3), the V_N level is further decreased to 0.55 eV above the VBM, whereas the N_i level is increased to 3.60 eV above the CBM. This implies that the levels have crossed due to the FP formation. In the crossing region (i.e., the eighth and ninth configurations in Fig. 3), however, it

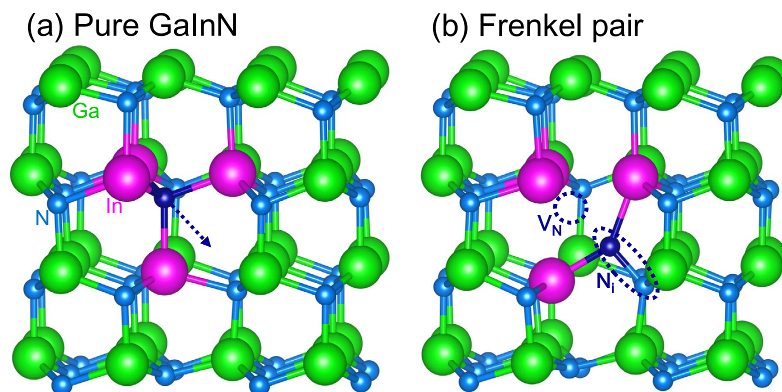

Figure 2. Atomic structure of (**a**) Pure InGaN and (**b**) with one FP defect. The moving N atom is denoted by a dark blue ball. In (**a**), arrow is the direction of the N displacement during the FP formation. In (**b**), split-interstitial and V_N are marked by dotted ellipse and circle, respectively.

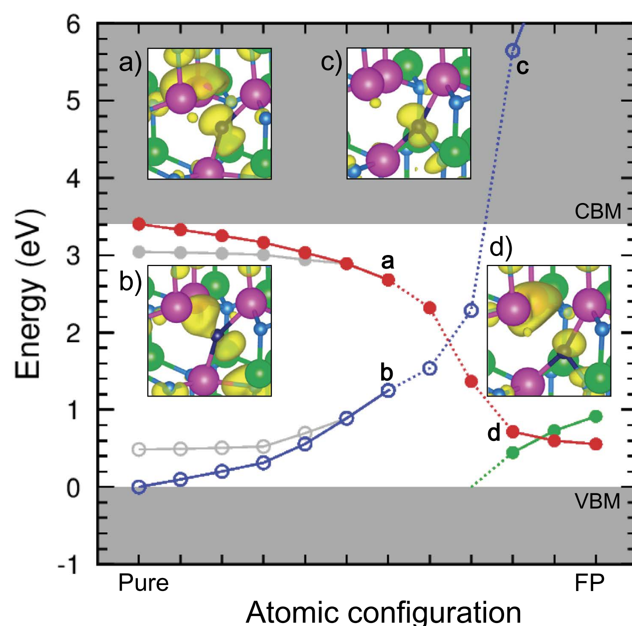

Figure 3. Change of energy level during FP formation with injected carriers. V_N and N_i levels are represented by red and blue lines, respectively. The filled (open) dot denotes fully occupied (empty) state. Dashed lines indicate the crossing region (explained in the text). Green line, popping up from VBM into the band gap, is another occupied N_i level. Insets are the charge density plots for the levels marked by a, b, c, and d. Gray lines are the uncorrected hybrid functional results.

happens that the constrained self-consistent field (SCF) calculation dose not converge. Nevertheless, we can see the level crossing indirectly by checking the charge densities at the tenth configuration, as shown in the insets in Fig. 3. In contrast to insets **a** and **b** where the lower-energy state has an N lone pair, insets **c** and **d** show that the lower-energy state has In dangling bonds, instead. Note that, for clarity, the issue of level crossing was not included in in Fig. 1, as this schematic figure depicts isolated defects for which the cation level is higher than the anion level.

The lack of convergence in the crossing region can be attributed to charge sloshing between the N_i and V_N states at each SCF step. A similar situation takes place in conventional DFT calculations, when two or more partially occupied levels are nearly degenerate. One may overcome the problem by smearing the occupation over a certain energy range. Here, before entering the crossing region, two electrons occupy the high-lying V_N level and two holes occupy the low-lying N_i level. After exiting the crossing region, the system is electronically de-excited, so no empty state is below occupied states. To assess the effect of this occupation change, we resort to fractional occupation, in particular, for the two interacting levels, labeled e_L and e_H, the following occupation numbers $(f_L, f_H) = (2 \times \frac{1}{3}, 2 \times \frac{2}{3})$ at the eighth configuration, and $(2 \times \frac{2}{3}, 2 \times \frac{1}{3})$ at the ninth configuration, are used. As expected, converged SCF results are obtained. To connect with the V_N and N_i levels in the

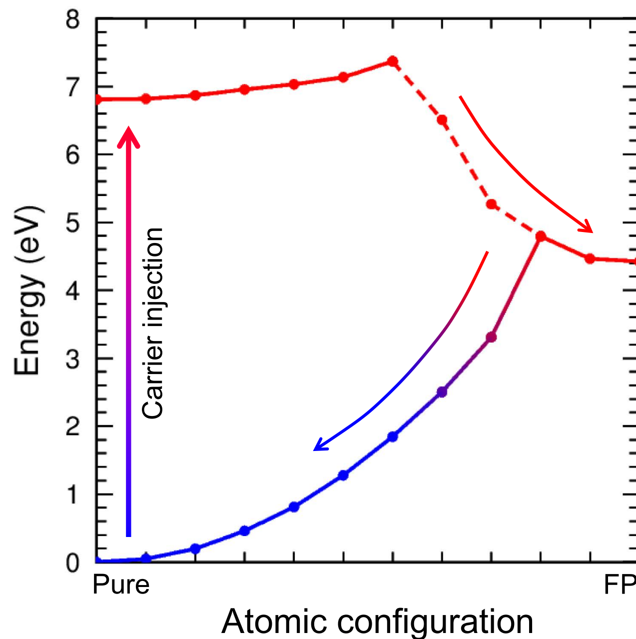

Figure 4. Potential energy curve in the NRR process. The FP formation and annihilation processes are corresponded to upper and lower lines, respectively. Red (blue) line is for the case where two electrons occupy the V_{N} (N_i) level. The changing color from-red-to-blue region is where the ground-state V_{N} and N_i levels couple to each other.

non-crossing regions in Fig. 3, we define an average energy $e_V = [f_H \cdot e_H + f_L \cdot e_L]/2$ for occupied V_{N} and $e_I = [(1 - f_H) \cdot e_H + (1 - f_L) \cdot e_L]/2$ for empty N_i. This yields smoothly connected energy levels between the excited and ground-state systems.

Potential energy curves in the NRR process. Figure 4 shows the potential energy manifold during the FP formation. By injecting two electrons and two holes in the CBM and VBM, respectively, the total energy of the system at the initial configuration is increased by twice of the band gap energy (6.81 eV). Here solid lines represent non-crossing regions whereas dashed lines represent the crossing region, as discussed above. The barrier for the FP formation, in the presence of carrier injection, is only 0.56 eV, which is significantly reduced from the 4.79 eV in the ground state. One can qualitatively understand the difference as follows: displacing an N from the defect-free structure increases the total energy of the system. However, the increase is substantially smaller than what would be in the ground state without the excitation, because the significant increase of the depleted N_i level no longer costs energy and the significant lowering of the occupied V_{N} level also helps to offset the energy required to break the bonds and associated strain. After forming the FP, the system will revert to the original defect-free structure, as it only needs to overcome a barrier of 0.47 eV.

We have analyzed the occupied energy level in the ground state during the reverse process back to the defect-free structure. It was found that the character of the occupied defect level is continuously changed from that of the V_{N} state to that of the N_i state. As the occupied N_i level and the empty V_{N} level eventually merge into the VB and CB, respectively, the NRR process assisted by carrier injection is completed. One may classify the transient defect mechanism in terms of a strong electron-phonon coupling, i.e., the significant energy level changes during the FP formation, and the reverse process transforms the initial excitation energy into thermal motion of the atoms.

Discussion

To see the dominate process in recombination, we compare the radiative recombination time of the excited carrier with the FP formation time. The FP annihilation process is, on the other hand, unimportant here because after the FP formation, the excited electrons already fall in a level lower than the holes (cf. Fig. 3) so that radiative recombination is no longer possible. We can estimate the FP formation time using the rate equation $r = 3 \times f\exp(-E_{\mathrm{b}}/k_{\mathrm{B}}T)$, where k_{B} is the Boltzmann constant, f is the optical phonon frequency, $2.0 \times 10^{13}\,\mathrm{s}^{-1}$ for GaN[25], E_{b} is the formation energy, 0.56 eV, and T is the junction temperature during the LED operation, 130 °C[26]. The factor 3 stands for the number of equivalent NRR pathways. The calculated NRR relaxation time is about 160 ns, which is about twice the radiative recombination time of 88 ns[27]. Over this time, about a quarter of the excited electrons undergo the NRR processes.

Note that the magnitude of the band gap is crucial for enabling the NRR process. When the band gap is smaller, the energy required to create two electron-hole pairs through carrier injection is also smaller, for example, in GaAs, it is only 2.84 eV, while the FP formation energy is 4.59 eV[28]. Therefore, no transient FP-formation can take place, even under the carrier injection condition.

Conclusion

Using density-functional theory calculations, we demonstrate the possible existence of a new NRR mechanism, where the injected high-energy carriers induce a structural instability, namely, the low-barrier transient defect formation, and the associated NRR through strong electron-phonon coupling. While our study is focused on GaN-based LEDs, the theory, as shown in Fig. 1, is general and could be an important limiting factor for other wide-gap semiconductors for the efficiency of their optoelectronic and photovoltaic devices. In particular, it raises the important question whether new mechanism(s) may exist between the widely-accepted defect-based SRH mechanism and the defect-free AR mechanism to account for some of the most difficult but technically important materials issues regarding excited carriers.

Methods

Our calculations are based on the density functional theory (DFT) with the Heyd–Scuseria–Ernzerhof screened hybrid exchange-correlation functional[29], as implemented in the VASP code[30]. We use a mixing parameter of 0.3 for the exact exchange, as in previous studies[31]. Projector augmented wave potentials[32,33] are used to represent ion cores. Plane waves with an energy cutoff of 306 eV and 230 eV are used as basis sets for InGaN and GaAs, respectively. We use a periodic supercell that contains 96 and 128 atoms to model the InGaN alloy and GaAs, respectively. Γ point is used for Brillouin zone sum. Atomic structures are relaxed until the residual forces are less than 0.03 eV/Å. To simulate electronic excitation, we perform constrained DFT calculations, in which we remove two electrons from the VB maximum (VBM) and place them at the CB minimum (CBM). Standard reaction-barrier-search algorithms, such as the nudged elastic band method, are not applicable to calculating the energy barrier in the present case, because electron occupation changes during the process. Instead, we generate ten intermediate configurations between the initial and final configurations and then relax all the atoms except for the diffusing N atom and a Ga atom of choice far away from the N.

References

1. Stoneham, A. M. Non-radiative transitions in semiconductors. *Rep. Prog. Phys.* **44,** 79 (1981).
2. Yang, J.-H., Shi, L., Wang, L.-W. & Wei, S.-H. Non-radiative carrier recombination enhanced by two-level process: a first-principles study. *Sci. Rep*. **6,** 21712 (2016).
3. Waltereit, P. *et al.* Nitride semiconductors free of electrostatic fields for efficient white light-emitting diodes. *Nature* **406,** 865–868 (2000).
4. Piprek, J. Efficiency droop in nitride-based light-emitting diodes. *Phys. Status Solidi A* **207,** 2217–2225 (2010).
5. Iveland, J. *et al.* Direct measurement of auger electrons emitted from a semiconductor light-emitting diode under electrical injection: identification of the dominant mechanism for efficiency droop. *Phys. Rev. Lett.* **110,** 177406 (2013).
6. Delaney, K. T., Rinke, P. & Van de Walle, C. G., Auger recombination rates in nitrides from first principles. *Appl. Phys. Lett.* **94,** 191109 (2009).
7. Meyaard, D. S. *et al.* Identifying the cause of the efficiency droop in GaInN light-emitting diodes by correlating the onset of high injection with the onset of the efficiency droop. *Appl. Phys. Lett.* **102,** 251114 (2013).
8. Kim, M.-H. *et al.* Origin of efficiency droop in GaN-based light-emitting diodes. *Appl. Phys. Lett.* **91,** 183507 (2007).
9. Chen, S. L., Chen, W. M., Ishikawa, F. & Buyanova, I. A. Suppression of non-radiative surface recombination by N incorporation in GaAs/GaNAs core/shell nanowires. *Sci. Rep*. **5,** 11653 (2015).
10. Nakamura, S. The roles of structural imperfections in InGaN-based blue light-emitting diodes and laser diodes. *Science* **281,** 956–961 (1998).
11. Shur, M. S. & Zukauskas, A. Solid-state lighting: toward superior illumination. *Proc. IEEE* **93,** 1691 (2005).
12. Tsao, J. Y. *et al.* Solid-state lighting: an energy-economics perspective. *J. Phys. D: Appl. Phys*. **43,** 354001 (2010).
13. Shockley, W. & Read, W. T. Statistics of the recombinations of holes and electrons. *Phys. Rev*. **87,** 835 (1952).
14. Hall, R. N. Electron-hole recombination in germanium. *Phys. Rev*. **87,** 387 (1952).
15. Du, M.-H., Branz, H. M., Crandall, R. S. & Zhang, S. B. Bistability-mediated carrier recombination at light-induced boron-oxygen complexes *in silicon*. *Phys. Rev. Lett.* **97,** 256602 (2006).
16. Zhang, S. B. & Branz, H. M. Nonradiative electron-hole recombination by a low-barrier pathway in hydrogenated silicon semiconductors. *Phys. Rev. Lett.* **84,** 967 (2000).
17. Wei, S.-H., Zhang, S. B. & Zunger, A. Off-center atomic displacements in zinc-blende semiconductor. *Phys. Rev. Lett.* **70,** 1639 (1993).
18. Siegal, Y., Glezer, E. N., Huang, L. & Mazur, E. Laser-induced phase transitions in semiconductors. *Annu. Rev. Mater. Sci.* **25,** 223–247 (1995).
19. Bang, J. *et al.* Regulating energy transfer of excited carriers and the case for excitation-induced hydrogen dissociation on hydrogenated graphene, *Proc. Natl. Acad. Sci. USA* **110,** 908–911 (2013).
20. Van de Walle, C. G. & Neugebauer, J. First-principles calculations for defects and impurities: applications to III-nitrides. *J. Appl. Phys.* **95,** 3851 (2004).
21. Xiao, H. Y., Zu, X. T., Gao, F. & Weber, W. J., Ab initio calculations of structural and energetic properties of defects in gallium nitride. *J. Appl. Phys.* **103,** 123529 (2008).
22. Using hybrid functional to study (delocalized) shallow states requires special attention because the long-range Hartree-Fock exchange can lead to unphysical change in the energy levels due to occupation change[22,23], which also affects the total energy of the system. As a result, the CBM state drops down by 0.36 eV whereas the VBM state moves up by 0.48 eV (see Fig. 3). This also lowers the system total energy by 0.73 eV.
23. Bang, J. *et al.* Difficulty in predicting shallow defects with hybrid functionals: implication of the long-range exchange interaction. *Phys. Rev. B* **88,** 035134 (2013).
24. Broqvist, P., Alkauskas, A. & Pasquarello, A. Hybrid-functional calculations with plane-wave basis sets: effect of singularity correction on total energies, energy eigenvalues, and defect energy levels. *Phys. Rev. B* **80,** 085114 (2009).
25. Saib, S., Bouarissa, N., Rodriguez-Hernandez, P. & Munoz Lattice vibration spectrum of GaN from first-principle calculations. A., *Semicond. Sci. Technol.* **24,** 025007 (2009).
26. Schwegler, V. *et al.* Ohmic heating of InGaN LEDs during operation: determination of the junction temperature and its influence on device performance. *Phys. Stat. Sol.* (*a*) **176,** 783–786 (1999).
27. Gladysiewicz, M. *et al.* Theoretical simulations of radiative recombination time in polar InGaN quantum wells. *Phys. Status Solidi C* **8,** 2273–2275 (2011).
28. In GaAs, our structural relaxation indicates that the As atom is displaced into the tetrahedral interstitial position.

29. Heyd, J., Scuseria, G. E. & Ernzerhof, M. Hybrid functionals based on a screened Coulomb potential. *J. Chem. Phys.* **118,** 8207 (2003).
30. Kresse, G. & Furthmuller, J. Efficiency of ab-initio total energy calculations for metals and semiconductors using a plane-wave basis set. *Comput. Mater. Sci.* **6,** 15–50 (1996).
31. Park, J.-S. & Chang, K. J. Diffusion and stability of hydrogen in Mg-doped GaN: A density functional study. *Appl. Phys. Express* **5,** 065601 (2012).
32. Blochl, P. E. Projector augmented-wave method. *Phys. Rev. B* **50,** 17953 (1994).
33. Kresse, G. & Joubert, D. From ultrasoft pseudopotentials to the projector augmented-wave method. *Phys. Rev. B* **59,** 1758 (1999).

Acknowledgements

This work was supported by the Department of Energy under Grant No. DE-SC0002623, NSF under Award No. DMR-1104994, the Basic Science Research Program through the National Research Foundation of Korea (NRF) funded by the Ministry of Science, ICT & Future Planning (NRF-2015R1C1A1A02037024), and KBSI grant C36117. The supercomputer time was provided by NERSC under DOE Contract No. DE-AC02-05CH11231 and the CCI at RPI.

Author Contributions

J.B. and S.B.Z. designed the research. Electronic structure calculations were performed by J.B. All authors were involved in the interpretation and discussion of the results. The paper was written by J.B. and S.B.Z. with contributions from all authors. S.B.Z. supervised the research.

Additional Information

Competing financial interests: The authors declare no competing financial interests.

How to cite this article: Bang, J. *et al.* Carrier-induced transient defect mechanism for non-radiative recombination in InGaN light-emitting devices. *Sci. Rep.* **6**, 24404; doi: 10.1038/srep24404 (2016).

This work is licensed under a Creative Commons Attribution 4.0 International License. The images or other third party material in this article are included in the article's Creative Commons license, unless indicated otherwise in the credit line; if the material is not included under the Creative Commons license, users will need to obtain permission from the license holder to reproduce the material. To view a copy of this license, visit http://creativecommons.org/licenses/by/4.0/